

## Parameterization of Land Surface Processes to Study Boundary Layer Characteristics over a Semiarid Region in Northwest India

A. N. V. SATYANARAYANA

*Department of Geography, National University of Singapore, Singapore*

V. N. LYKOSOV

*Institute of Numerical Mathematics, Russian Academy of Sciences, Moscow, Russia*

U. C. MOHANTY

*Centre for Atmospheric Sciences, Indian Institute of Technology, New Delhi, India*

E. E. MACHUL'SKAYA

*Institute of Numerical Mathematics, Russian Academy of Sciences, Moscow, Russia*

(Manuscript received 1 October 2001, in final form 30 September 2002)

### ABSTRACT

The atmospheric boundary layer and land surface processes play a crucial role and affect large-scale phenomena such as monsoons. A comprehensive soil-vegetation parameterization scheme has been developed to understand the complex interaction of the transfer processes, such as heat and moisture within the atmospheric surface layer and the active land layer. In this scheme, attention is given to the accurate representation of soil heat and moisture by considering all three states of water and their phase transitions. This scheme is incorporated in a one-dimensional multilevel boundary layer model for accurate representation of energy exchange processes to study the boundary layer characteristics. Numerical experiments are carried out with this model using special datasets obtained from the Land Surface Processes Experiment (LASPEX-97) at Anand (22.4°N, 72.6°E), a semiarid region of the state of Gujarat in northwest India. For this study, a dry simulation in February 1997 and a wet situation in July 1997 are considered. The model-simulated temporal variation of the fluxes of sensible heat, latent heat, and net radiation and soil temperatures are compared with the available observations. The results suggest that this model is suitable for better representation of land surface processes and the PBL in large-scale atmospheric models.

### 1. Introduction

The coupling of land surface processes with the upper layers of the atmosphere occurs through exchange of momentum, heat, and moisture. The exchange processes in the atmospheric surface layer and soil are the result of complex interactions. The role of land surface processes in the simulation of atmospheric circulation is examined by various land surface parameterization schemes. The importance of land surface characteristics in generating mesoscale circulations has also been recognized in recent years. Zhang and Anthes (1982) demonstrated that variations in soil moisture could cause significant effects on the boundary layer characteristics. This requires a proper parameterization of soil-vegetation processes over the land surface to be incorporated in an atmospheric boundary layer model that will im-

prove the characterization of the boundary layer processes. Proper parameterization of subgrid-scale boundary layer processes is gaining in importance in the large-scale weather forecasting models (Mahfouf et al. 1987; Stull and Driedonks 1987; Holt and Raman 1988). Soil and vegetation characteristics play a vital role in modifying the surface energy balance and thus influence planetary boundary layer (PBL) processes (Mihailović et al. 1993; Sellers et al. 1986; Noilhan and Planton 1989; Volodin and Lykosov 1998). Recent reviews by Garratt (1993), Bougeault (1991), Blondin (1991), Rowntree (1991), Avissar and Verstraete (1990), and Laval (1988) include different methods of representing the land surface processes in NWP and climate models. Dickinson et al. (1991) and Sellers (1992) studied the role of the biosphere in controlling the evapotranspiration and Xue et al. (1991) employed a simplified biosphere model for global climate studies.

Raman et al. (1998) investigated the influence of soil moisture and vegetation in simulating monsoon circulation and rainfall by incorporating a simple land surface

---

*Corresponding author address:* Prof. U. C. Mohanty, Centre for Atmospheric Sciences, Indian Institute of Technology, Delhi, Hauz Khas, New Delhi 110 016, India.  
E-mail: mohanty@cas.iitd.ernet.in

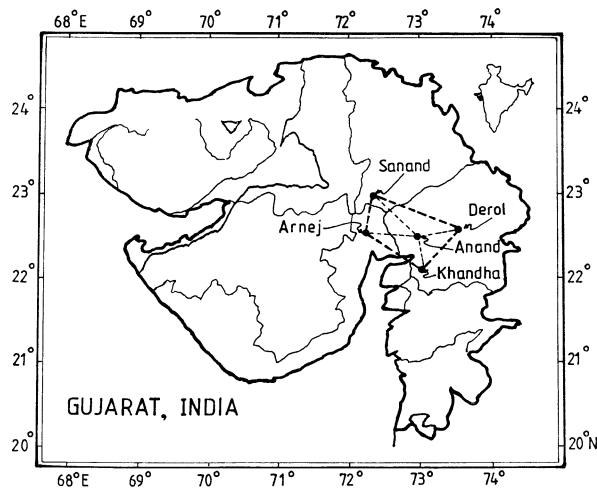


FIG. 1. Regional map of the study area.

parameterization scheme in a three-dimensional, high-resolution, regional, nested-grid, atmospheric model. Very few studies have been conducted on land surface processes in India. To fill this gap, a multi-institutional Land Surface Processes Experiment (LASPEX-97) funded by the Department of Science and Technology, Government of India, was conducted by Indian Institute of Tropical Meteorology (IITM), Pune, and Gujarat Agriculture University, Anand, over the Sabarmati basin area in 1997. Satyanarayana et al. (2000) have studied the atmospheric boundary layer characteristics during winter at Anand. Nagar et al. (2000) studied the evolution of the atmospheric boundary layer at Anand during the boreal summer month of May.

In the present study an attempt has been made to simulate the boundary layer characteristics using a one-dimensional PBL model with the turbulent kinetic energy (TKE)–dissipation ( $e-\epsilon$ ) closure scheme and a single-column comprehensive soil–vegetation parameterization scheme model with LASPEX-97 datasets over a semiarid region, Anand (22.4°N, 72.6°E), in the state of Gujarat in the northwest India during February 1997 (dry case) and July 1997 (wet case). A regional map of the study area is given in Fig. 1. The prime objective of this study is to develop and validate a model of an interacting boundary layer and a soil–vegetation system for use in limited-area models for monsoon forecasting.

## 2. Data

Micrometeorological tower data were used from a tower at Anand located in the midst of an agriculture farm within the Gujarat Agriculture University campus. This region is a flat river basin area situated in the semiarid/arid zone of the western part of India. This region falls in the wheat zone of India and has a homogeneous terrain. Low-level crops were grown during the experimental period. A wheat crop was grown during February 1997 and sun hemp in July 1997. Advection components are found

to be small over this area as verified by NCMRWF (National Centre for Medium-Range Weather Forecasting) large-scale analyses. The conditions are well suited for applying a one-dimensional/single-column model to understand the land surface processes and boundary layer characteristics at Anand.

In the study, Intensive Observation Period (IOP) data during 14–17 February (dry case) and 13–17 July 1997 (wet case) at Anand consisted of tower as well as upper-air [radiosonde/rawinsonde (RS/RW)] observations. The data consisted of temperature, wind speed, and wind direction at 1-, 2-, 4-, and 8-m heights; relative humidity at 2- and 4-m heights from the 9-m tower; and surface pressure. Upper-air observations of temperature, dew-point temperature, wind speed, and wind direction at different pressure levels up to 700 hPa were used. Vegetation parameters such as leaf area index, vegetation cover, soil type and texture, soil temperature at the surface, 5-, 10-, 20-, 40-, and 100-cm depth, soil moisture, incoming solar radiation, reflected incoming solar radiation, upward longwave radiation and downward longwave radiation, net radiation, and soil heat flux at 5-cm depth were used.

Data obtained from sonic anemometers were also used. Two types of sonic anemometers were used in the field experiment. One is an Applied Technology three-axis sonic anemometer, and the other is a Metek three-axis sonic anemometer. The data obtained from these sonic anemometers were zonal wind component ( $\text{m s}^{-1}$ ), meridional wind component ( $\text{m s}^{-1}$ ), vertical velocity ( $\text{m s}^{-1}$ ), and temperature ( $^{\circ}\text{C}$ ) with a sampling interval of 10 Hz. The Metek anemometer has a built-in processor that analyzes the wind and temperature data and evaluates the surface-layer parameters such as momentum flux, sensible heat flux, and friction velocity using eddy correlation technique. These parameters were evaluated after averaging the data for 10 min. In this study these direct measurements were used.

## 3. Model formulation

In this section the details of the soil–vegetation heat and moisture transfer scheme and the one-dimensional PBL model with  $e-\epsilon$  closure scheme are given. These two models are combined and employed to study the atmospheric boundary layer processes and the impact of the land surface processes.

### a. Soil–vegetation heat and moisture transfer scheme

In the mathematical representation of soil heat and moisture transfer, all physical processes are assumed to be one-dimensional, because the vertical gradients of temperature and moisture in its various states are larger than their horizontal gradients. The heat and moisture transfer processes are due to diffusion and are interconnected.

To compute the soil surface temperature, the following surface heat budget equation is used:

$$R_n = H_s + LE_s + G, \quad (1)$$

where  $R_n$  is surface net radiation flux ( $\text{W m}^{-2}$ ),  $H_s$  is sensible heat flux ( $\text{W m}^{-2}$ ),  $LE_s$  is latent heat flux ( $\text{W m}^{-2}$ ), and  $G$  is soil heat flux ( $\text{W m}^{-2}$ ). Subscript  $s$  denotes surface.

The soil heat and moisture transfer equations, with plant roots taken into account, can be written as follows (Volodin and Lykossov 1998):

$$\rho C \frac{\partial T}{\partial t} = \frac{\partial}{\partial z} \lambda_T \frac{\partial T}{\partial z} + \rho(L_i F_i - L_v F_v) \quad (2)$$

$$\frac{\partial W}{\partial t} = \frac{\partial}{\partial z} \lambda_w \left( \frac{\partial W}{\partial z} + \delta \frac{\partial T}{\partial z} \right) + \frac{\partial \gamma}{\partial z} - F_i - F_v - R_f - R_r \quad (3)$$

$$\frac{\partial V}{\partial t} = \frac{\partial}{\partial z} \lambda_v \frac{\partial V}{\partial z} + F_v \quad (4)$$

$$\frac{\partial I}{\partial t} = F_i. \quad (5)$$

Here,  $t$  is the time (s);  $z$  is the downward vertical coordinate (m);  $T$  is the soil temperature ( $^{\circ}\text{C}$ );  $W$  is the soil liquid water content equal to the mass of soil liquid water per unit mass of dry soil ( $\text{kg kg}^{-1}$ );  $V$  is the water vapor content ( $\text{kg kg}^{-1}$ );  $I$  is the ice content ( $\text{kg kg}^{-1}$ );  $\lambda_T$  is the heat conductivity ( $\text{J m}^{-1} \text{K}^{-1} \text{s}^{-1}$ );  $\lambda_w$  and  $\lambda_v$  are the diffusivities of liquid water and water vapor, respectively ( $\text{m}^2 \text{s}^{-1}$ );  $\delta$  is the moisture conductivity due to the temperature gradient ( $\text{K}^{-1}$ );  $\rho$  is the soil density ( $\text{kg m}^{-3}$ );  $C$  is the soil heat capacity ( $\text{J kg}^{-1} \text{K}^{-1}$ );  $\gamma$  is the rate of water infiltration due to gravity ( $\text{m s}^{-1}$ );  $F_i$  is the rate of change in the liquid water and ice content due to melting and freezing ( $\text{s}^{-1}$ );  $F_v$  is the rate of change in water vapor and liquid water content due to evaporation and condensation ( $\text{s}^{-1}$ );  $L_i$  is the latent heat of freezing/melting ( $\text{J kg}^{-3}$ );  $L_v$  is the latent heat of evaporation/condensation ( $\text{J kg}^{-1}$ );  $R_f$  is the runoff ( $\text{s}^{-1}$ ); and  $R_r$  is the rate of water uptake by the plant roots ( $\text{s}^{-1}$ ). Equations (2)–(5) are solved within the layer (0,  $H$ ), where  $H = 100$  cm and is the soil level to which the intraseasonal temperature variations extend. Total number of modeled soil layers chosen in the model is 40.

The numerical implementation of the scheme is based on a second-order-accurate finite-difference scheme for the spatial derivatives and a first-order-accurate implicit scheme for the time derivatives. The integration of the scheme is split into two substeps at every time step. The diffusion equations are solved at the first half-step, with the matrix factorization procedure used to invert a block three-diagonal matrix. At the second half-step, the temperature and moisture profile are adjusted by computing the sources and sinks involved in (2)–(5) (see Volodin and Lykossov 1998).

The total heat capacity of the soil is assumed to depend on the water content:

$$C = C_g + C_w W, \quad (6)$$

where  $C_g$  and  $C_w$  are the specific heat ( $\text{J kg}^{-1} \text{K}^{-1}$ ) of dry and wet soil, respectively. The heat conductivity is calculated by using the following relation given by McCumber and Pielke (1981):

$$\lambda_T = 418.68 \max[\exp(-P_f - 4.7), 0.00041], \quad (7)$$

where  $P_f = \log_{10}(-\psi)$  and  $\psi$  is the soil water potential in meters.

The soil water potential, the water diffusivity, and the hydraulic fluxes are computed following the relation given by Clapp and Hornberger (1978):

$$\psi = \psi_{\max} \left( \frac{W_{\max}}{W} \right)^b, \quad \lambda_w = \lambda_{\max} \left( \frac{W}{W_{\max}} \right)^{b+2},$$

$$\gamma = \gamma_{\max} \left( \frac{W}{W_{\max}} \right)^{2b+3}, \quad (8)$$

where  $b$  is a dimensionless parameter (Clapp–Hornberger's constant). The hydraulic flux going out across the lower boundary is considered to be the subsurface runoff. A max subscript denotes quantities at the maximum soil water capacity, which is determined by  $W_{\max} = \Pi/\rho$ , where  $\Pi$  is the soil porosity. Both  $\Pi$  and  $\rho$  are dependent on the soil type. The soil type of the study area is loamy sand. Soil heat flux ( $G$ ) can be computed using the following relation:

$$G = -\lambda_T \frac{\partial T}{\partial z} \quad \text{at } z = 0.$$

#### b. Vegetation and evaporation from the land surface

In this scheme, while representing the heat and moisture transfer in the soil–vegetation system, we have not taken into account the aerodynamic properties of plants. The main emphasis is on evaporation. It is assumed that a grid square occupied by land can include bare and inland water areas as well as areas with dry and wet vegetation of various types. When the moisture flux  $E$  ( $\text{kg m}^{-2} \text{s}^{-1}$ ) due to evaporation is calculated, it is assumed that the surface temperature and other atmospheric parameters do not depend on the type of underlying surface. Following DKRZ (1992), we have

$$E = \rho_a \sum_{i=1}^N \mu_i (q_i - q_a) / R_i, \quad (9)$$

where  $\mu_i$  is the fraction of the grid square covered by the surface of the  $i$ th type;  $q_i$  ( $\text{kg kg}^{-1}$ ) and  $q_a$  ( $\text{kg kg}^{-1}$ ) are the effective humidity at the ground surface and air, respectively;  $\rho_a$  ( $\text{kg m}^{-3}$ ) is the density of air; and  $R_i$  ( $\text{m}^{-1} \text{s}$ ) is the resistance. For wet vegetated and water-covered surfaces  $q_i$  ( $\text{kg kg}^{-1}$ ) is equal to the saturation specific humidity at the surface temperature,  $q_{\max}(T_s)$ . For bare soils,  $q_i$  is calculated following DKRZ (1992), as follows:

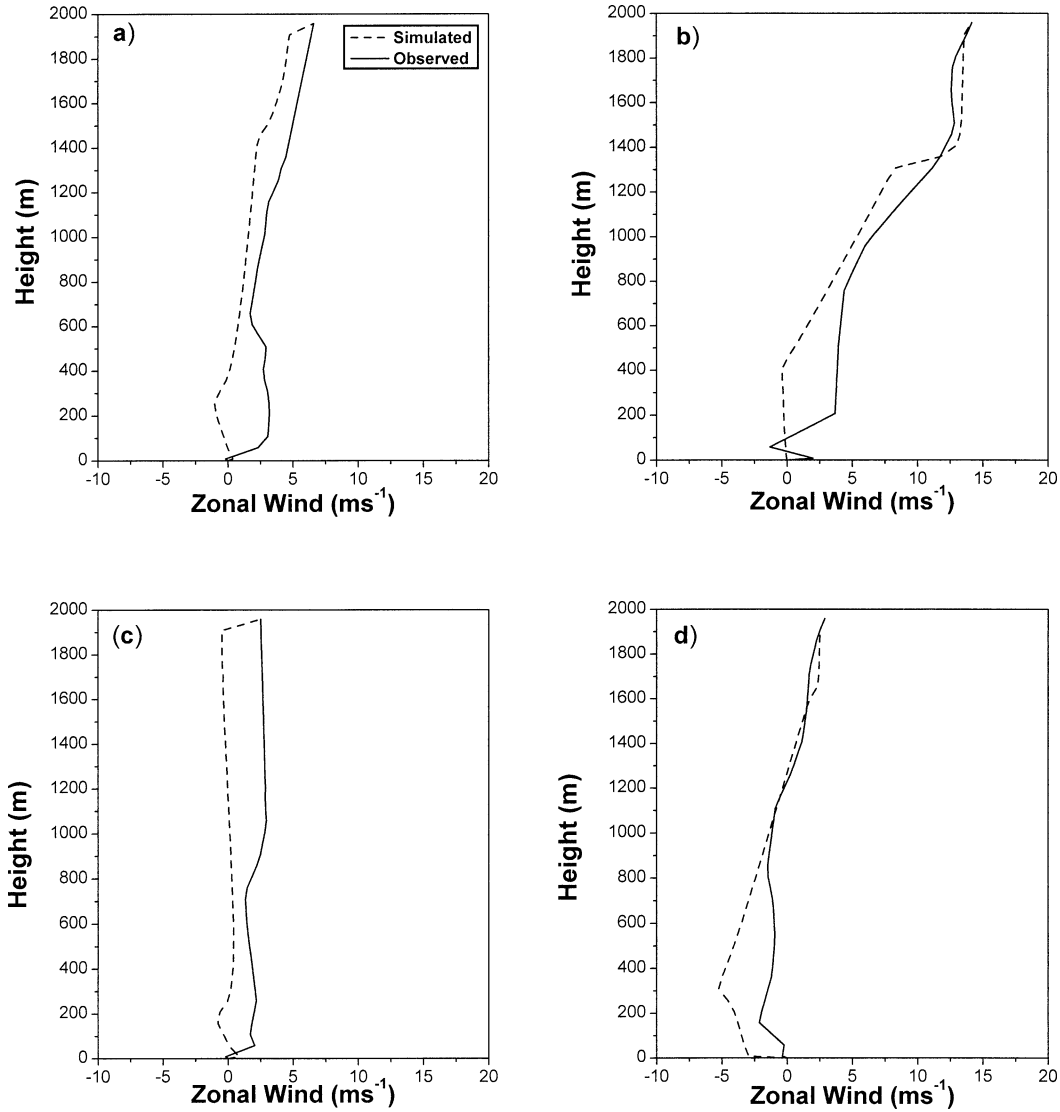


FIG. 2. Observed and simulated vertical profiles of zonal wind ( $m s^{-1}$ ) at (a) 0000 UTC and (b) 0600 UTC 15 Feb and (c) 0000 UTC and (d) 0600 UTC 17 Feb 1997.

$$\frac{q_i}{q_{max}} = \max \left[ \frac{1}{2} \left( 1 - \cos \frac{\pi W_s}{W_{s,max}} \right), \min \left( 1, \frac{q_a}{q_{max}} \right) \right]. \quad (10)$$

In both cases,  $R_i = 1/C_T U$ , where  $U$  is the absolute value of the wind velocity at the atmospheric model level next to the ground surface and  $C_T$  is the coefficient of heat and moisture exchange.

For dry vegetation, it is also assumed that  $q_i = q_{max}$  but the resistance  $R_i$  (Sellers et al. 1986) is defined as

$$R_i = \frac{1}{C_T U} + \frac{R(S_{ph})}{F_T F_q F_w}, \quad (11)$$

where

$$\frac{1}{R(S_{ph})} = \frac{1}{kc} \left[ \frac{b_i}{d_i S_{ph}} \ln \left( \frac{d_i e^{kLt} + 1}{d_i + 1} \right) - \ln \left( \frac{d_i + e^{-kLt}}{d_i + 1} \right) \right]$$

and

$$d_i = \frac{a_i + b_i c_i}{c_i S_{ph}}, \quad k = 0.9. \quad (12)$$

Here  $S_{ph}$  is the fraction of the shortwave net radiation  $S$  utilized in photosynthesis;  $a_i$ ,  $b_i$ , and  $c_i$  are parameters dependent on the vegetation type; and  $Lt$  is the leaf area index (LAI). The function  $F$  determines the dependence of the resistance on air temperature and humidity and soil moisture content (Sellers et al. 1986),

$$F_T = 1 - C_{FT} (T_b - T_a)^2,$$

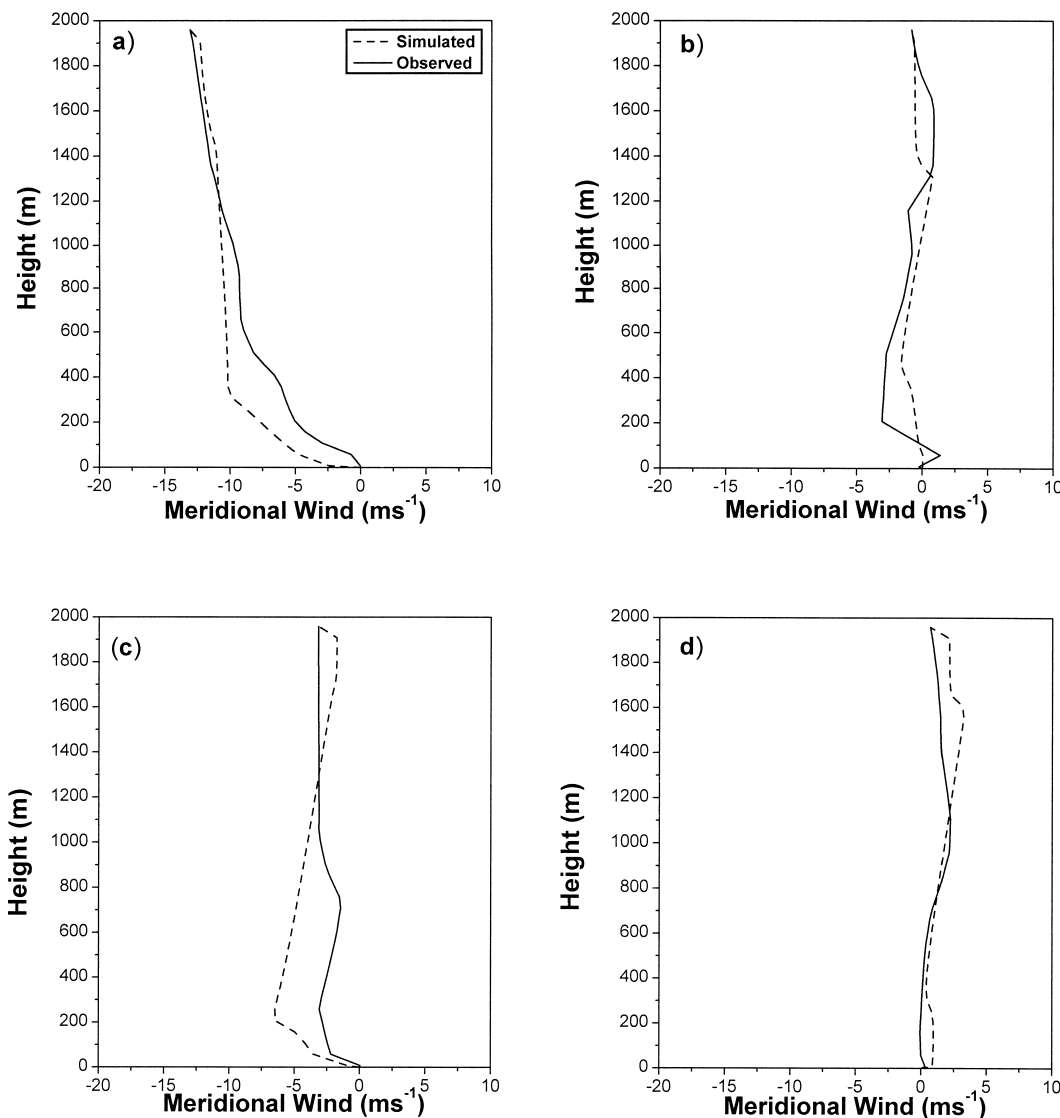


FIG. 3. Observed and simulated vertical profiles of meridional wind ( $m s^{-1}$ ) at (a) 0000 UTC and (b) 0600 UTC 15 Feb and (c) 0000 UTC and (d) 0600 UTC 17 Feb 1997.

$$\begin{aligned}
 F_q &= 1 - C_{Fq}(q_{max} - q_a)^2, \\
 F_w &= \frac{W_r - W_w}{W_b - W_w},
 \end{aligned}
 \tag{13}$$

where  $C_{FT} = 0.0016 K^{-1}$ ,  $T_b = 298.15 K$ , and  $C_{Fq}$  depends on the vegetation type. The value  $W_b$  is the soil water content at which the plants begin to wilt,  $W_w$  is the soil water content at the wilting point, and  $W_r$  is the actual water content at the soil levels within the root zone. The following relations are used in the model:

$$W_r = \sum_{k=1}^{k_r} W_k \rho_{rk} \nabla z_k,$$

$$\begin{aligned}
 W_b &= \sum_{k=1}^{k_r} \left( \frac{\Pi}{\rho} \right)_k \left( \frac{\psi_b}{\psi_{max}} \right)_k^b \rho_{rk} \nabla z_k, \\
 W_w &= \sum_{k=1}^{k_r} \left( \frac{\Pi}{\rho} \right)_k \left( \frac{\psi_w}{\psi_{max}} \right)_k^b \rho_{rk} \nabla z_k,
 \end{aligned}
 \tag{14}$$

where  $k_r$  is the soil-level number corresponding to the deepest roots,  $\rho_r$  is the density of the roots,  $\psi_b$  is the soil water potential at which the plants begin to wilt, and  $\psi_w$  is the soil water potential at which the plant is already wilted. The soil water content is limited as  $W_w < W < W_b$ . The maximum water amount contained in the root zone is determined in a similar way:

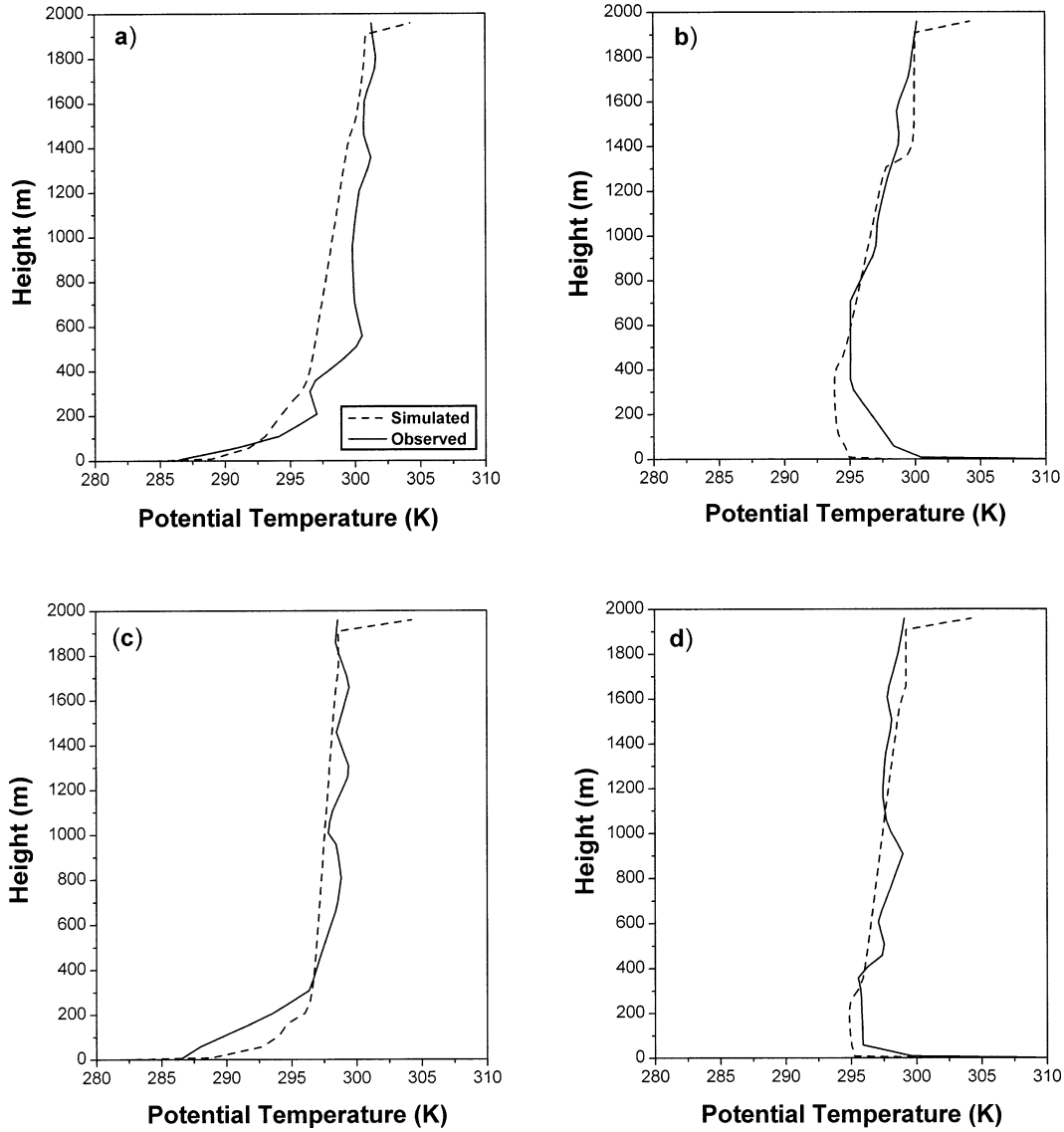


FIG. 4. Observed and simulated vertical profiles of potential temperature (K) at (a) 0000 UTC and (b) 0600 UTC 15 Feb and (c) 0000 UTC and (d) 0600 UTC 17 Feb 1997.

$$W_{S,max} = \sum_{k=1}^{k_r} \left( \frac{\Pi}{\rho} \right)_k \rho_{rk} \nabla z_k. \quad (15)$$

The fractional vegetation coverage and LAI are the prescribed seasonally dependent input parameters of the model.

*c. One-dimensional PBL model with 1.5-order e-ε closure scheme*

In a Cartesian coordinate system, where the horizontal axes  $x$  and  $y$  are directed in the east and north, respectively, and the vertical axis  $z$  is directed upward, the planetary boundary layer equations can be written in the following form (Lykossov and Platov 1992; Satyanarayana et al. 2000):

$$\frac{\partial u}{\partial t} = -\frac{\partial \overline{u'w'}}{\partial z} + fv + \frac{\tilde{p}_x}{\tilde{\rho}}, \quad (16)$$

$$\frac{\partial v}{\partial t} = -\frac{\partial \overline{v'w'}}{\partial z} - fu - \frac{\tilde{p}_y}{\tilde{\rho}}, \quad (17)$$

$$\frac{\partial \theta}{\partial t} + u\tilde{\theta}_x + v\tilde{\theta}_y = -\frac{\partial \overline{\theta'w'}}{\partial z} + Q_r + Q_f, \quad (18)$$

$$\frac{\partial q}{\partial t} + u\tilde{q}_x + v\tilde{q}_y = -\frac{\partial \overline{q'w'}}{\partial z} + E_p - C, \quad (19)$$

$$\frac{\partial q_w}{\partial t} + u\tilde{q}_{wx} + v\tilde{q}_{wy} = -\frac{\partial \overline{q'_w w'}}{\partial z} - E_p + C - P, \quad (20)$$

where  $u$  ( $m s^{-1}$ ),  $v$  ( $m s^{-1}$ ), and  $w$  ( $m s^{-1}$ ) are  $x$ ,  $y$ , and  $z$  components of the wind velocity;  $\theta$  (K) is the potential

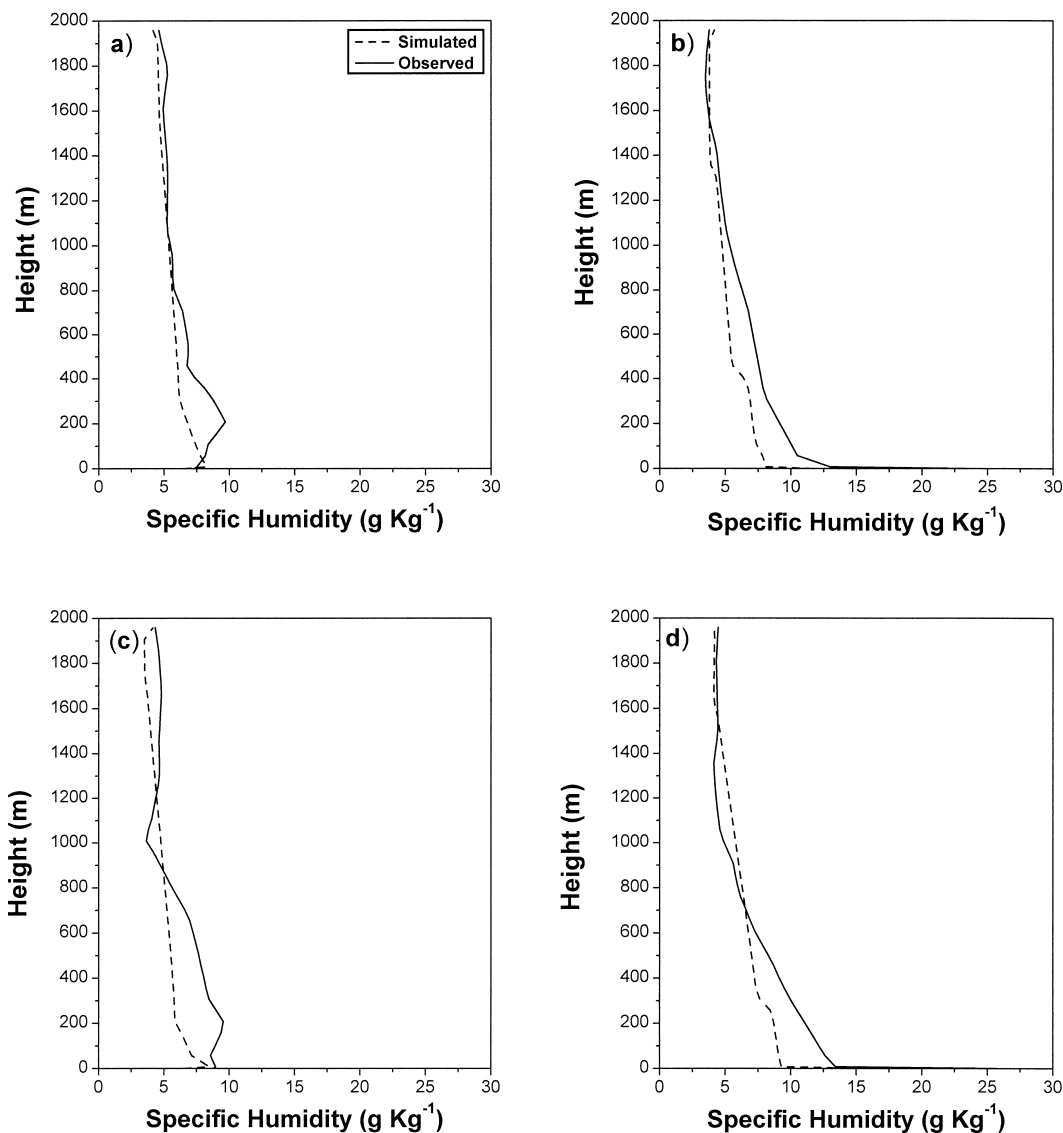


FIG. 5. Observed and simulated vertical profiles of specific humidity ( $\text{g kg}^{-1}$ ) at (a) 0000 UTC and (b) 0600 UTC 15 Feb and (c) 0000 UTC and (d) 0600 UTC 17 Feb 1997.

temperature;  $q$  ( $\text{kg kg}^{-1}$ ) is the specific humidity;  $q_w$  ( $\text{kg kg}^{-1}$ ) is the specific liquid water content;  $\rho$  ( $\text{kg m}^{-3}$ ) is the density of the air–water–water vapor mixture;  $(\bar{p}_x, \bar{p}_y)$ ,  $(\bar{\theta}_x, \bar{\theta}_y)$ ,  $(\bar{q}_x, \bar{q}_y)$  are components of horizontal gradients of the pressure, potential temperature, specific humidity, and specific liquid water content in the free atmosphere;  $Q_r$  and  $Q_f$  are rates of the heat change due to radiation and phase transitions of the water;  $C$  and  $E_p$  are rates of phase changes: water vapor to liquid water and water to water vapor;  $P$  is the precipitation rate;  $u'w'$ ,  $v'w'$ ,  $\theta'w'$ ,  $q'w'$ , and  $q'_w w'$  are the vertical turbulent fluxes of momentum, heat, water vapor and liquid water; and  $f$  is the Coriolis parameter.

In this model, the horizontal pressure gradients are computed using geostrophic wind relationships (Sayanarayana et al. 2000). To compute the radiative flux-

es, the radiation scheme developed by Harshavardhan et al. (1987) is implemented in the model.

The above set of PBL equations are derived from the governing equations considering the large-scale flow as well as the perturbations in the boundary layer, following Gutman (1972) to represent the smooth transmission of boundary layer processes' smooth transition from mixed layer into the free atmosphere.

In order to calculate vertical turbulent fluxes of momentum, heat, and moisture in the interfacial layer, the Boussinesq hypothesis is used:

$$\overline{a'w'} = -K_a \frac{\partial a}{\partial z},$$

where  $a$  is any of the prognostic variables, namely,  $u$ ,

$v$ ,  $w$ ,  $\theta$ ,  $q$ ,  $q_w$ ;  $K_a$  is the eddy exchange coefficient. It is assumed that  $K_a = \alpha_a K$ , where  $\alpha_a$  is a dimensionless constant (equals to unity for the momentum flux). The coefficient  $K$  is related to the turbulent kinetic energy ( $e$ ) and the dissipation ( $\epsilon$ ) as given by Kolmogorov (1942):

$$K_a = \frac{C_k e^2}{\epsilon},$$

where  $C_k$  is a dimensionless constant.

To calculate the turbulence kinetic energy and dissipation rate, the following additional equations are used:

$$\frac{\partial e}{\partial t} = \left( -\overline{u'w'} \frac{\partial u}{\partial z} + \overline{v'w'} \frac{\partial v}{\partial z} + \frac{g}{\rho} \overline{\rho'w'} + \epsilon \right) - \frac{\partial \overline{w'E'}}{\partial z}, \quad (21)$$

$$\begin{aligned} \frac{\partial \epsilon}{\partial t} = & -C_1 \frac{\epsilon}{E} \left( -\overline{u'w'} \frac{\partial u}{\partial z} + \overline{v'w'} \frac{\partial v}{\partial z} + \frac{g}{\rho} \overline{\rho'w'} + \epsilon \right) \\ & - \frac{\partial \overline{w'\epsilon'}}{\partial z}, \end{aligned} \quad (22)$$

where  $C_1$  is a function depending on  $Re = (2e/3)^2/\nu e$  (see Satyanarayana et al. 2000). Here,  $\nu$  is the air molecular viscosity.

#### d. Boundary conditions

The prescribed values of temperature and specific humidity at the soil bottom of the model are used as lower boundary conditions.

The interfacial layer is kept as the maximum height of the constant flux layer ( $h = 8$  m). The boundary conditions then, for the prognostic variables at the constant flux layer height,  $z = h$ , are as follows:

$$K \frac{\partial u}{\partial z} = C_D |\mathbf{V}_h| u_h, \quad (23)$$

$$K \frac{\partial v}{\partial z} = C_D |\mathbf{V}_h| v_h, \quad (24)$$

$$\frac{H_s}{C_p \rho} = K_\theta \frac{\partial \theta}{\partial z} = -C_\theta |\mathbf{V}_h| (\theta_h - \theta_s), \quad (25)$$

$$\frac{E_s}{\rho} = K_\theta \frac{\partial q}{\partial z} = -C_\theta |\mathbf{V}_h| (q_h - q_s), \quad (26)$$

where  $H_s$  and  $LE_s$  are the sensible and latent heat fluxes at the land surface, the subscript  $h$  indicates that the corresponding quantities refer to the upper boundary of the constant flux layer, and the subscript  $s$  refers to the quantities determined at the air–soil interface. In (23) to (26) we have used the notation  $\mathbf{V} = (u, v)$ . The surface layer is treated in the light of Monin and Obukhov similarity theory (Satyanarayana et al. 2000).

The maximum height of the turbulent boundary layer (top of the boundary layer, 1958 m) is chosen as the upper boundary. At the top of the boundary layer, the wind speeds, the potential temperature, and the moisture attain the observed values at that height. The TKE and dissipation flux are assumed to vanish at that height.

In fact, it is an iterative procedure at each time step. Assuming the surface temperature is known, the surface fluxes are computed and used as lower boundary conditions for the PBL model; from the surface heat budget equation, soil heat flux is calculated and used as the upper boundary condition for the soil, and finally we have the new surface temperature.

## 4. Numerical experiment

The initial conditions are prepared using the 0300 UTC RS/RW balloon data of 14 February 1997 for the dry case and 0000 UTC data of 13 July 1997 for the wet case at Anand. The initial values at model grid points are obtained by linearly interpolating the high-resolution vertical profile data, which consist of zonal and meridional wind components, temperature, and specific humidity. The interpolated values of these parameters at every 50 m in the vertical from 8 m (assumed height of the constant flux layer height) to 1958 m (top of the model domain) are given as the input to the model. At the height of constant flux layer, the observations from the micrometeorological tower are prescribed.

For comparing the computed surface temperatures with the measurements, 3-hourly surface and micrometeorological tower observations at Anand, which consisted of surface temperature, surface pressure, and surface relative humidity, are used. The time variation of these boundary conditions at every time step was obtained by linear interpolation in time. The observations at the top of the model domain were also interpolated in time and prescribed as upper boundary conditions. The subsurface boundary conditions for the soil–vegetation heat and moisture transportation model, such as soil bot-

TABLE 1. Details of soil and vegetation parameters used in the study.\*

Month	Vegetation type	Vegetation cover fraction	Soil moisture (g g <sup>-1</sup> )	LAI	Crop under the tower
Feb 1997	Cultivated land with ground cover	0.3	0.04	3.0	Wheat
Jul 1997	Cultivated land with ground cover	0.8	0.27	3.0	Sun hemp

\* Soil type = loamy sand; bulk density =  $1.55 \times 10^{-3}$  km m<sup>-3</sup>; thermal conductivity =  $0.944$  W m<sup>-1</sup> K<sup>-1</sup>; thermal diffusivity =  $0.508 \times 10^{-6}$  m<sup>2</sup> s<sup>-1</sup>.

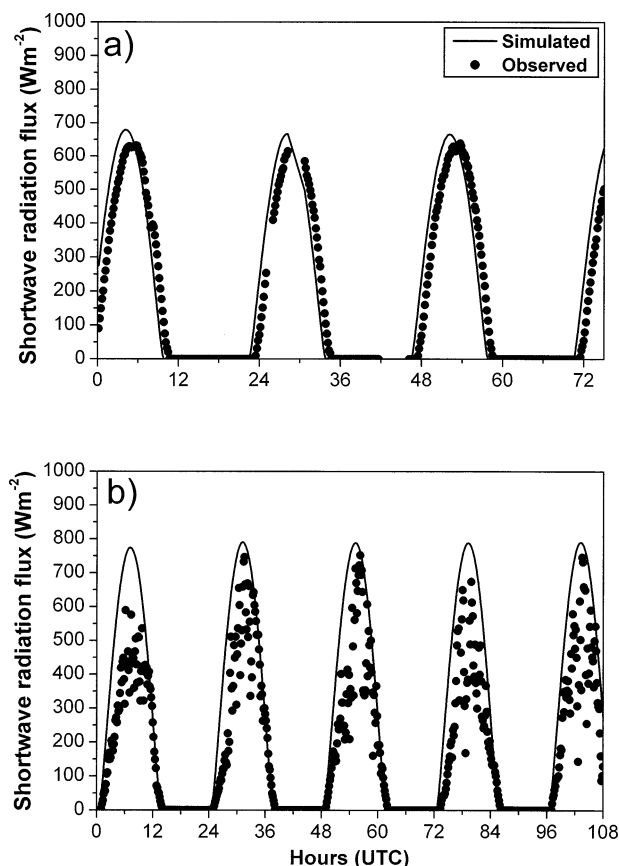


FIG. 6. Temporal variation of shortwave radiation flux ( $\text{W m}^{-2}$ ) along with the observations during (a) 0300 UTC 14 Feb–0300 UTC 17 Feb and (b) 0000 UTC 13 Jul–1200 UTC 17 Jul 1997.

tom temperature and specific humidity, are obtained from the observations. Details of soil and vegetation parameters used in the study are given in Table 1. The model was integrated for 75 h for the dry case and for 108 h for the wet case with a time step of 600 s.

## 5. Results and discussion

The model results consist of the simulations of vertical profiles of zonal and meridional components of wind, potential temperature, and specific humidity at Anand. The model also generated sensible heat, latent heat, shortwave radiation, net radiation and soil heat fluxes and boundary layer height for both dry and wet cases. The simulations are compared with the available observations. The observed profiles of zonal and meridional wind components, potential temperature, and specific humidity obtained from RS/RW observations are linearly interpolated in the vertical and values at every 50-m interval up to 2000 m were used for comparison.

To see the performance of the model in simulating vertical profiles of zonal and meridional wind components, potential temperature, and specific humidity, the

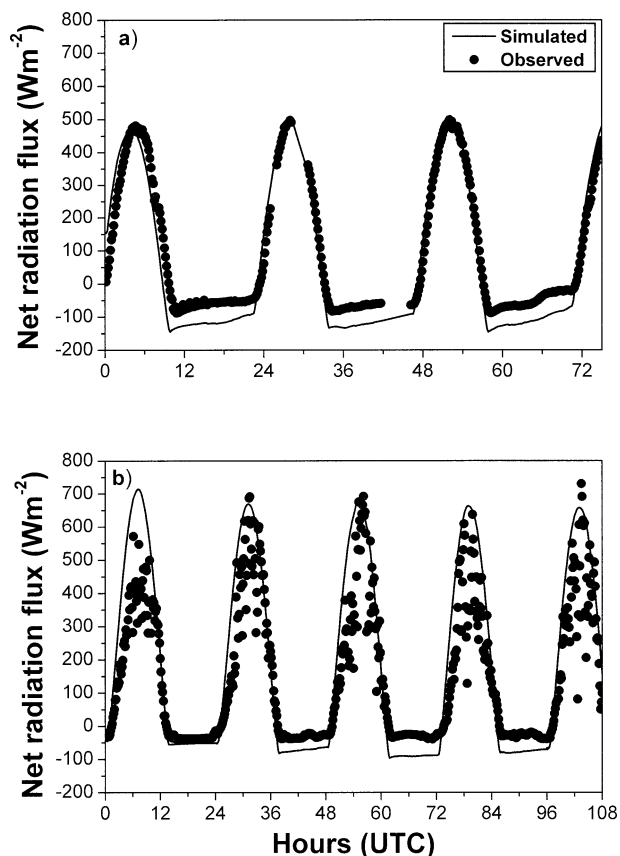


FIG. 7. Temporal variation of net radiation flux ( $\text{W m}^{-2}$ ) along with the observations during (a) 0300 UTC 14 Feb–0300 UTC 17 Feb and (b) 0000 UTC 13 Jul–1200 UTC 17 Jul 1997.

results obtained from the dry case are presented. The model was able to simulate the vertical profiles of the preceding parameters reasonably well (not shown).

The vertical profiles of model simulations and observations of zonal and meridional wind components on 15 February at 0000 and 0600 UTC and on 17 February at 0000 and 0600 UTC are depicted in Figs. 2a–d and 3a–d. The model was able to simulate these components reasonably well with little deviations in the surface layer.

The potential temperature profiles for the same period mentioned earlier are presented in Figs. 4a–d. The model captured the superadiabatic lapse rate conditions very well as seen in the observations depicted in Figs. 4b,d. The stable stratification is also simulated very well as seen in Figs. 4a,c. A steep gradient is noticed both in stable as well as unstable stratifications from observations and simulations. A strong inversion of  $\sim 12.5$  K is noticed in the observations (Figs. 4a,c). The model was able to simulate the intensity of the stable layer as well as the unstable layer reasonably well.

The model simulations against the observations of specific humidity profiles are presented in Figs. 5a–d. Over the entire model simulations are found to be in good comparison with the observations.

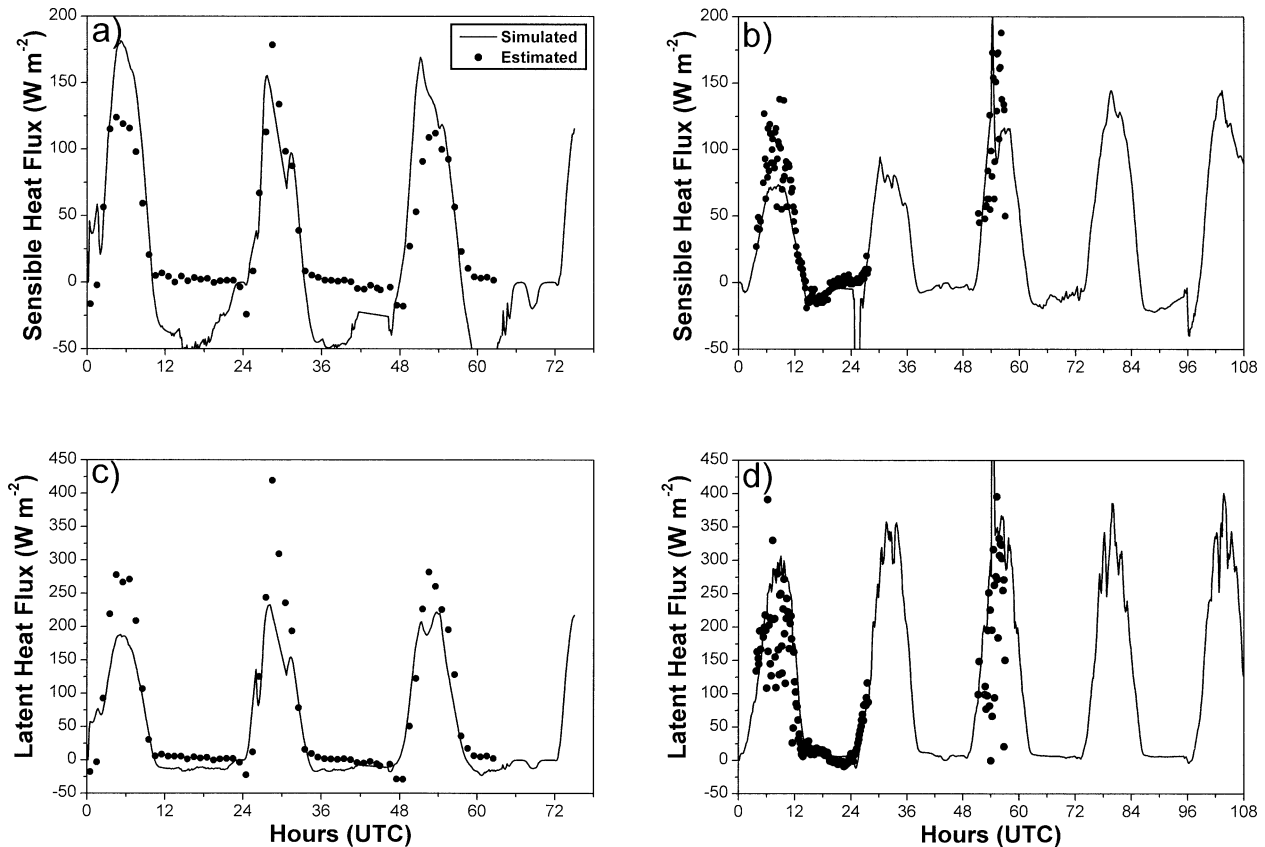


FIG. 8. Temporal variation of sensible heat flux ( $\text{W m}^{-2}$ ) during (a) 0300 UTC 14 Feb–0300 UTC 17 Feb and (b) 0000 UTC 13 Jul–1200 UTC 17 Jul and latent heat flux ( $\text{W m}^{-2}$ ) during (c) 0300 UTC 14 Feb–0300 UTC 17 Feb and (d) 0000 UTC 13 Jul–1200 UTC 17 Jul 1997 along with the observations.

Figures 6a,b represent the diurnal and day-to-day variation of shortwave radiation flux for the dry and wet cases, respectively. During the dry case (Fig. 6a), it is noticed that model was able to simulate the diurnal pattern well. But the time of occurrence of the peak value is shifted by an hour from the observations, when compared with the model simulations. During the wet case (Fig. 6b), the model was able to reproduce the diurnal cycle as well as the time of occurrence of the peak value well. During 13 and 16 July, the model overpredicted the flux whereas during 14, 15, and 17 July it did well.

The diurnal and day-to-day variation of net radiation flux is presented in Figs. 7a,b, for the dry and wet cases, respectively. Interestingly, the model simulations almost coincide with the observations in the dry case and wet case. It is seen that the model was better able to reproduce the net radiation flux during the daytime than at night, when compared with the observations.

Figures 8a–d represent the model simulations of diurnal variation of sensible heat flux during February and July and latent heat flux during February and July, along with the observations/estimations, respectively. A maximum simulated sensible heat fluxes of  $\sim 180$ ,  $\sim 150$ , and  $\sim 170 \text{ W m}^{-2}$  are simulated on 14, 15, and 16 February (Fig. 8a), whereas the maximum estimated

fluxes are  $\sim 125$ ,  $\sim 180$ , and  $125 \text{ W m}^{-2}$ . Even though the model slightly underpredicts the sensible heat flux, the time of occurrence of the maximum flux and the diurnal pattern are represented very well. It is also noticed that the model overpredicted the negative sensible heat flux during nighttime in the period of the study. This could be due to strong coupling between the air and ground during the nighttime. In this study radiation fluxes are computed using the calculated vertical profiles of temperature and humidity along with the reference profiles (standard atmospheric profiles) above the PBL. During the night there is no solar flux and errors in temperature and humidity profiles above the PBL could lead to errors in the net surface radiation and to strong coupling. Under unstable stratification during the day, there is sufficient solar flux and, hence, these errors are not as significant. Also, as stated by Derbyshire (1999), in stable stratification, boundary layer decoupling can occur in idealized single-column models, which leads to this kind of inconsistency. During the wet case (Fig. 8b), the model was able to simulate the diurnal as well as day-to-day variation of the sensible heat flux. The simulations are compared with the instantaneous observations obtained from the sonic anemometer. The gaps are due to the nonavailability of the observations.

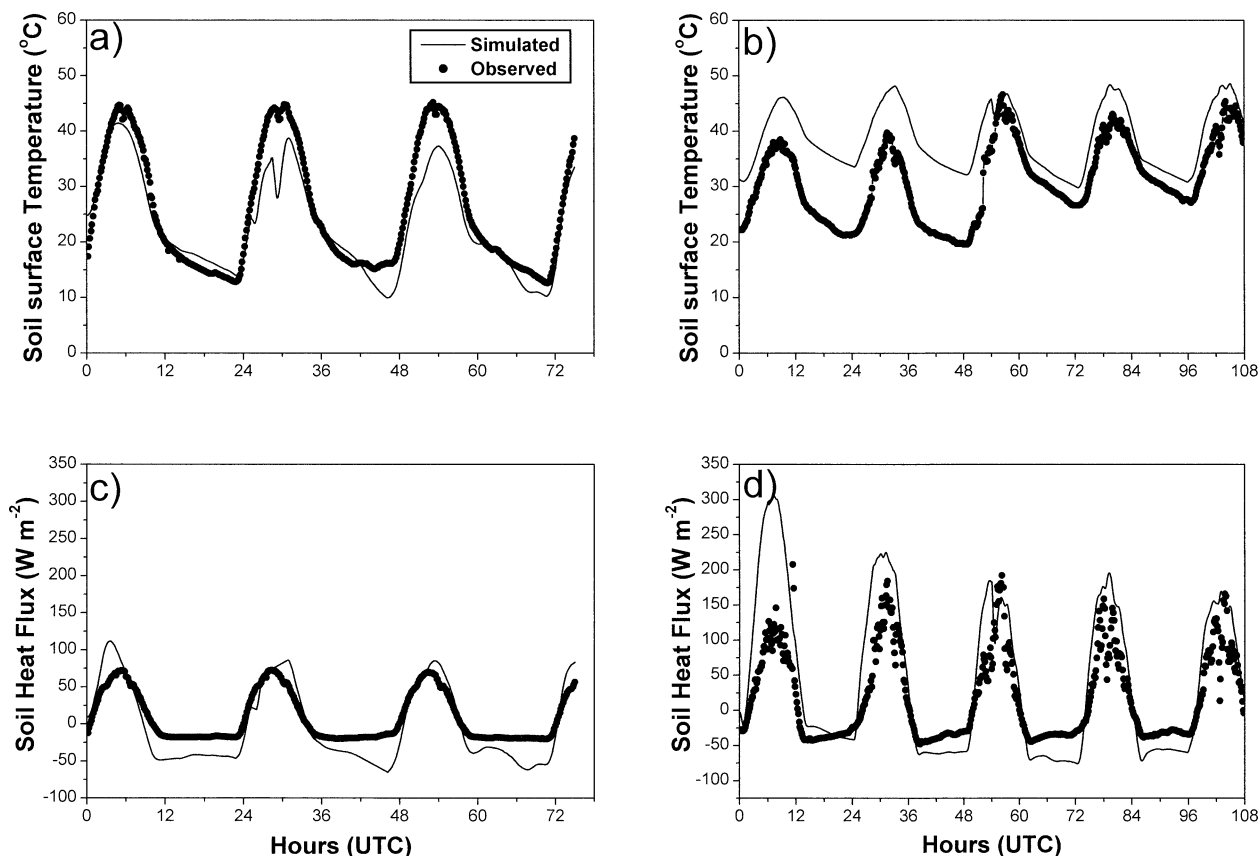


FIG. 9. Temporal variation of surface soil temperature ( $^{\circ}C$ ) during (a) 03 UTC 14 Feb–0300 UTC 17 Feb and (b) 0000 UTC 13 Jul–1200 UTC 17 Jul and soil heat flux ( $W m^{-2}$ ) during (c) 0300 UTC 14 Feb–0300 UTC 17 Feb and (d) 0000 UTC 13 Jul–1200 UTC 17 Jul 1997 along with the observations.

The model underpredicted the flux on 13 July. One can see that the model-simulated flux is less than  $100 W m^{-2}$  on 13 and 14 July, whereas it is more than  $125 W m^{-2}$  on 15, 16, and 17 July. This may be attributed to the underestimation of the surface soil temperature simulations during 13 and 14 July and will be discussed in the following sections. In general, the model was able to simulate the sensible heat flux during the dry and wet case well.

Maximum latent heat fluxes of  $\sim 190$ ,  $\sim 230$ , and  $225 W m^{-2}$  are simulated on 14, 15, and 16 February. The model simulations are compared with the estimated values (bulk aerodynamic method) due to the nonavailability of the direct observations. It is seen that the model was able to reproduce the diurnal as well as the day-to-day variation of the latent heat flux well. For the wet case, maximum simulated latent heat fluxes of  $\sim 300$ ,  $\sim 350$ ,  $\sim 450$ ,  $\sim 380$ , and  $\sim 400 W m^{-2}$  are noticed. The simulation of the latent heat flux is compared with the estimated values. Using the surface energy balance, the latent heat flux values for the wet case are estimated, as instantaneous observations of the sensible heat flux, net radiation flux, and soil heat flux were available. The gaps in these estimations are due to the

absence of any one of the components of the surface energy balance. The model simulations are in the good agreement with the estimated values. One can discern the difference between the dry and wet case in the magnitude of the latent heat flux and to some extent in the sensible heat flux values. The model was able to simulate the different characteristic features of the dry and wet cases.

The diurnal and day-to-day variations of soil surface temperature during the dry case are depicted in Fig. 9a. A clear-cut diurnal and day-to-day variation is observed. The model underestimated the maximum soil temperature on 15 and 16 February, whereas the magnitude as well as the occurrence of the minimum soil temperature is simulated well. It is noticed that the simulation curve shows the same amplitude as noticed in the observations. Figure 9b represents the simulation of soil surface temperature and its diurnal as well day-to-day variations. It is seen that, in general, the diurnal variation of the soil temperature is reproduced well in the simulations in comparison to the observations. It is found that during 13 and 14 July the maximum observed soil surface temperature is around  $38^{\circ}C$  and from 15 July it is noted to be around  $45^{\circ}C$ . This situation is not simulated

well. It is also noticed that the amplitude of the diurnal variation curve is much less (both in observations as well as simulations) in comparison with the dry case (both in simulations as well as observations). It may be attributed to the presence of more soil moisture in the upper levels of the soil during July than in the February case.

Figures 9c,d depict the soil heat flux simulation along with the observed values. Results indicate the successful simulation of the soil heat flux during both cases in comparison with the observations. As expected, during the dry case the maximum observed soil heat flux is around  $75 \text{ W m}^{-2}$  whereas it is around  $225 \text{ W m}^{-2}$  during the wet case. More diurnal amplitude of soil heat flux is noticed in the case of July (both in simulations and observations) than in the case of February. It is just a reversal to the surface soil temperature simulations (Figs. 9a,b).

## 6. Sensitivity experiment

To study the performance of the comprehensive soil-vegetation heat and moisture transfer model with a one-dimensional PBL model ( $e-\epsilon$  closure), sensitivity experiments are conducted. In the present study, sensitivity of soil moisture in simulating the sensible heat flux, soil surface temperature, and soil heat flux during the wet case are presented in Figs. 10a–c. In this experiment the vegetation cover is fixed at 0.8 (80% of the area is covered with vegetation) and the model is integrated with different soil moisture values. It is noted that the magnitude as well as the amplitude of the diurnal curve is diminished when the soil moisture started increasing from the observed value to near the field capacity. At a particular time, that is, at 0300 UTC on 14 July, the maximum value of sensible heat flux rose to  $150 \text{ W m}^{-2}$  when the soil moisture value was  $0.04 \text{ g g}^{-1}$  and then decreased to  $\sim 75 \text{ W m}^{-2}$  when the prescribed soil moisture value was  $0.12 \text{ g g}^{-1}$ . The flux became almost negligible when the soil moisture value was near to the field capacity value. A similar kind of variation is noticed in the soil surface temperature simulations. As the soil moisture increased, the diurnal amplitude of the soil surface temperature curve also diminished. In the case of soil heat flux the reverse is noticed. As the soil moisture increases the soil heat flux also increased. This experiment reveals the sensitivity of the model in simulating the important surface energy components, which have direct influence on the surface layer processes and in turn affect boundary layer characteristics.

## 7. Conclusions

From the results of the numerical experiments carried out in this study, the following broad conclusions may be drawn. The model simulations of profiles of zonal and meridional wind components, potential temperature, and specific humidity are in good agreement with the

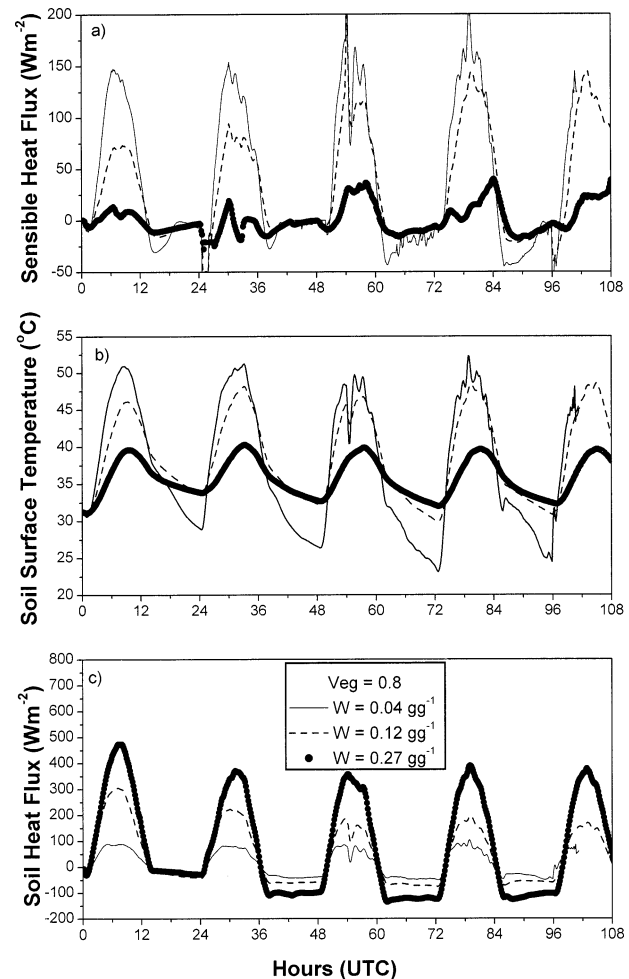


FIG. 10. Sensitivity experiment: temporal variation of (a) sensible heat flux ( $\text{W m}^{-2}$ ), (b) surface soil temperature ( $^{\circ}\text{C}$ ) and (c) soil heat flux ( $\text{W m}^{-2}$ ) during 0000 UTC of 13 Jul–1200 UTC of 17 Jul 1997 for different values of soil moisture ( $\text{g g}^{-1}$ ) by keeping vegetation cover constant.

observations. The model was able to capture the unstable stratification much better than the stable stratification. More detailed studies are needed to study the PBL under stable stratification by improving the turbulence closure and radiation transfer in the present scheme. Higher values of sensible heat flux are found in the dry case than in the wet case, whereas the reverse is noticed in latent heat flux. Higher values of soil heat flux are noticed in the wet case than in the dry case. The diurnal as well as day-to-day variations of soil temperature is reproduced better by the model in the dry case than in the wet case. Sensitivity experiments show the importance of soil moisture in simulating the crucial parameters, such as the sensible heat flux, soil heat flux, and soil surface temperature that have a direct impact in modifying the surface layer and the boundary layer processes, which subsequently affect the large-scale features. These results encourage the use of this model for

better representation of PBL and land surface processes in large-scale models.

*Acknowledgments.* The authors gratefully acknowledge the Department of Science and Technology, Government of India and Russian Academy of Sciences for the financial support to carry out the study. The authors also thank Dr. G. B. Pant, Director, IITM, Pune, BL&LSPS Group of IITM, and India Meteorological Department (IMD), New Delhi, for providing the necessary datasets. The authors are indebted to the anonymous referees for their helpful comments. This work has been partially supported from the Project INTAS 00-189 and by the Russian Fund for Basic Research (Grant 01-05-64150).

#### REFERENCES

- Avissar, R., and M. M. Verstraete, 1990: The representation of continental surface processes in atmospheric models. *Rev. Geophys.*, **28**, 35–52.
- Blondin, C., 1991: Parameterization of land surface processes in numerical weather prediction. *Land Surface Evaporation: Measurement and Parameterization*, T. J. Schmugge and J. C. Andre, Eds., Springer-Verlag, 31–54.
- Bougeault, P., 1991: Parameterization of land surface processes in numerical weather prediction. *Land Surface Evaporation: Measurement and Parameterization*, T. J. Schmugge, and J. C. Andre, Eds., Springer-Verlag, 55–92.
- Clapp, R. B., and G. M. Hornberger, 1978: Empirical equations for some soil hydraulic properties. *Water Resour. Res.*, **14**, 601–604.
- Derbyshire, S. H., 1999: Boundary-layer decoupling over cold surfaces as a physical boundary-instability. *Bound.-Layer Meteor.*, **90**, 297–325.
- Dickinson, R. E., A. Henderson-Sellers, C. Rosenzweig, and P. J. Sellers, 1991: Evapotranspiration models with canopy resistance for use in climate models: A review. *Agric. For. Meteorol.*, **54**, 373–388.
- DKRZ, 1992: The ECHAM3 atmospheric general circulation model. Tech. Rep. 6, Deutsches Klimazentrum, Hamburg, Germany, 188 pp.
- Garratt, J. R., 1993: Sensitivity of climate simulations to land surface and atmospheric boundary layer treatments—a review. *J. Climate*, **6**, 419–449.
- Gutman, L. N., 1972: *Introduction to the Non-linear Theory of Mesoscale Meteorological Processes*. Keter Press, 224 pp.
- Harshvardhan, D. Roger, D. A. Randall, and T. G. Corsetti, 1987: A fast radiation parameterization for atmospheric circulation models. *J. Geophys. Res.*, **92**, 1009–1016.
- Holt, T., and S. Raman, 1988: A review of comparative evaluation of multilevel boundary layer parameterizations for first-order and turbulent kinetic energy closure schemes. *Rev. Geophys.*, **26**, 761–780.
- Kolmogorov, A. N., 1942: Incompressible fluid turbulent motion equations. *Izv. Akad. Nauk SSSR, Ser. Fiz.*, **6**, 56–58.
- Laval, K., 1988: Land surface processes. *Physically-Based Modelling and Simulation of Climate and Climatic Change—Part I*, M. E. Schlesinger, Ed., Kluwer Academic, 285–306.
- Lykossov, V. N., and G. A. Platov, 1992: A numerical model of interaction between atmospheric and oceanic boundary layers. *Russ. J. Numer. Anal. Math. Modell.*, **7**, 419–440.
- Mahfouf, J. F., E. Richard, P. Mascart, E. C. Nickerson, and R. Rosset, 1987: A comparative study of various parameterizations of the planetary boundary layer in a numerical mesoscale model. *J. Climate Appl. Meteorol.*, **26**, 1671–1695.
- McCumber, M. C., and R. A. Pielke, 1981: Simulation of the effects of the surface fluxes of heat and moisture in a mesoscale numerical model. Part 1: Soil layer. *J. Geophys. Res.*, **86**, 9929–9938.
- Mihailović, D. T., R. A. Pielke, B. Rajković, T. J. Lee, and M. Jeftić, 1993: A resistance representation of schemes for evaporation from bare and partly plant-covered surfaces for use in atmospheric models. *J. Appl. Meteorol.*, **32**, 1038–1054.
- Nagar, S. G., A. Tyagi, P. Seetaramayya, and S. S. Singh, 2000: Evolution of an atmospheric boundary layer at a tropical semi-arid station, Anand, during boreal summer month of May—a case study. *Curr. Sci.*, **78**, 595–600.
- Noilhan, J., and S. Planton, 1989: A simple parameterization of land surface processes for meteorological models. *Mon. Wea. Rev.*, **117**, 536–549.
- Raman, S., U. C. Mohanty, N. C. Reddy, K. Alapaty, and R. V. Madala, 1998: Numerical simulation of the sensitivity of summer monsoon circulation and rainfall over India to land surface processes. *Pure Appl. Geophys.*, **152**, 781–809.
- Rowntree, P. R., 1991: Parameterization of land surface processes in numerical weather prediction. *Land Surface Evaporation: Measurement and Parameterization*, T. J. Schmugge and J. C. Andre, Eds., Springer-Verlag, 5–29.
- Satyanarayana, A. N. V., V. N. Lykossov, and U. C. Mohanty, 2000: A study on atmospheric boundary layer characteristics at Anand, India, using LSP experimental data sets. *Bound.-Layer Meteorol.*, **96**, 393–419.
- Sellers, P. J., 1992: Biophysical models of land surface processes. *Climate System Modelling*, K. E. Trenberth, Ed., Cambridge University Press, 451–490.
- , Y. Minth, Y. C. Sud, and A. Dalchar, 1986: A Simple Biosphere Model (Sib) for use within general circulation models. *J. Atmos. Sci.*, **43**, 505–531.
- Stull, R. B., and A. G. M. Driedonks, 1987: Applications of the transitional turbulent parameterization to atmospheric boundary layer simulations. *Bound.-Layer Meteorol.*, **40**, 209–239.
- Volodin, E. M., and V. N. Lykossov, 1998: Parameterization of heat and moisture transfer in the soil-vegetation system for use in atmospheric general circulation model. 1. Formulation and simulations based on local observational data. *Izv. Atmos. Ocean Phys.*, **34**, 453–465.
- Xue, Y., P. J. Sellers, J. C. Kinter, and J. Shukla, 1991: A simplified biospheric model for global climate studies. *J. Climate*, **4**, 345–364.
- Zhang, D., and R. A. Anthes, 1982: A high-resolution model of the planetary boundary layer—sensitivity tests and comparisons with SESAME-79 data. *J. Appl. Meteorol.*, **21**, 1594–1609.